Journal of Molecular Spectroscopy 300 (2014) 131–138

Contents lists available at ScienceDirect

Journal of Molecular Spectroscopy

journal homepage: www.elsevier.com/locate/jms

The Boltzmann constant from the shape of a molecular spectral line

A. Castrillo, L. Moretti, E. Fasci, M.D. De Vizia, G. Casa, L. Gianfrani *

Dipartimento di Matematica e Fisica, Seconda Università di Napoli, Viale Lincoln 5, I-81100 Caserta, Italy

ARTICLE INFO

Article history:
Available online 13 April 2014

Keywords:
High resolution spectroscopy
Spectral line shapes
Fundamental metrology
Boltzmann constant

ABSTRACT

We report on our recent determination of the Boltzmann constant, k_B, by means of Doppler broadening thermometry. This relatively new method of primary gas thermometry was implemented by using a pair of offset-frequency locked extended-cavity diode lasers at 1.39 μm, to probe a particular vibration–rotation transition of the $H_2^{18}O$ molecule. Adopting a rather sophisticated and extremely refined line shape model in the spectral analysis procedure, we were able to determine the Doppler width from high-quality absorption spectra with unprecedented accuracy. Our spectroscopic determination of k_B exhibits a combined (type A plus type B) uncertainty of 24 parts over 10^6. The complete uncertainty budget is presented and discussed.

1. Introduction

As is well known, the Boltzmann constant is the basic constant of statistical mechanics and thermodynamics, appearing in several fundamental laws of physics. It was introduced by Planck to provide the link between Boltzmann's statistical definition of entropy and the conventional one [1]. Boltzmann himself never introduced it, as he never thought to the possibility of carrying out an exact measurement of the constant [2]. Boltzmann, whose studies on entropy date back to 1870, could not imagine that roughly hundred and forty years later the Boltzmann constant (k_B) would have been the subject of tremendous efforts in the attempt to measure it with an uncertainty better than one part over 10^6.

The renewed interest towards k_B arises from the possible redefinition of the International System of Units (SI). In fact, the International Committee for Weights and Measures (CIPM) has proposed new definitions for the kilogram, ampere, kelvin, and mole, based upon the assignment of fixed numerical values to a set of fundamental constants, namely Planck constant, elementary charge, Boltzmann constant, and Avogadro number [3]. The changes proposed for the SI units will be adopted only after a further refinement of the experimental results on these constants. A refined value of k_B should ideally be determined by at least three different methods, at a combined uncertainty of 1 part per million (ppm) or better [4]. Presently, the most accurate way to access the value of k_B is from measurements of the speed of sound in a noble gas (Ar) inside an acoustic resonator. After over 40 years of research and technical developments, acoustic gas thermometry has recently provided a k_B determination with a relative uncertainty of 0.71 parts over 10^6 [5]. Another consolidated approach, based upon the Clausius–Mossotti equation, deals with measurements of the electric susceptibility of helium as a function of the gas pressure. Dielectric constant gas thermometry has recently led to a k_B value with a combined uncertainty of 4.3 ppm [6]. Other upcoming primary thermometry techniques are currently at the stage of further development and optimization. Among them, the newest and most promising one is Doppler broadening thermometry (DBT).

The expression of the Doppler width of a given atomic or molecular spectral line, valid for a gaseous sample at the thermodynamic equilibrium, namely $\Delta\omega_D = \frac{\omega_0}{c}\sqrt{2ln2\frac{k_BT}{M}}$, being ω_0 the line center frequency, c the speed of light, and M the molecular mass, represents a powerful tool to link the thermodynamic temperature, T, to an absolute frequency and a frequency interval, passing through the Avogadro number and the Boltzmann constant [7]. Therefore, DBT consists in retrieving the Doppler width from the highly-accurate observation of the profile corresponding to a given atomic or molecular line in a gas sample at the thermodynamic equilibrium. If implemented at the temperature of the triple point of water (namely, 273.16 K), pursuing the highest levels of precision and accuracy for laser absorption spectroscopy in the linear regime of interaction, DBT provides an optical determination of the Boltzmann constant.

In proof-of-principle experiments, performed on NH_3 and CO_2 molecules, k_B was determined with a combined uncertainty of 190 and 160 ppm, respectively [8,9]. The ammonia infrared spectrum was probed by a frequency-stabilized CO_2 laser at 10.34 μm, while an extended-cavity diode laser (ECDL) at 2 μm was used to interrogate a vibration–rotation transition of carbon

* Corresponding author. Fax: +39 0823274714.
E-mail address: livio.gianfrani@unina2.it (L. Gianfrani).

http://dx.doi.org/10.1016/j.jms.2014.04.001
0022-2852/

dioxide. At that time, the spectral analysis was performed by using either Gaussian or Voigt profiles [10,11].

In the last few years, with the ambitious goal of approaching the target accuracy of 1 ppm, technical improvements of the experimental setups have been accompanied by a more and more refined interpolation of the absorption line shapes, also involving other molecular targets, such as water [12]. Particularly, a great attention has been paid to the role of line narrowing effects.

It is well known that molecular line shapes exhibit clear deviations from the time honoured Voigt profile. Even in the case of a well isolated spectral line, under the influence of binary collisions, the shape can be quite complicated by the joint occurrence of Dicke narrowing and speed-dependent effects. In 2011, for the $H_2^{18}O$ spectrum at 1.38 μm, we demonstrated that the molecular confinement alone is unable to explain entirely the departures from the Voigt profile and that the speed dependence of pressure-induced broadening and shifting cannot be ignored, even in the case of pure water samples in the Doppler regime [13,14]. In fact, absorption spectra were successfully interpolated, under the soft collision approximation, using the uncorrelated version of the speed-dependent Galatry profile, with a hypergeometric dependence on the absorber speed for both pressure broadening and shifting parameters, thus reaching an agreement between theory and experiment at the level of 5×10^{-5} [13]. More recently, we have also tested the quadratic approximation in the speed dependence of relaxation rates, demonstrating the partial failure of the so-called quadratic speed-dependent models [15,16]. Simultaneously, the partially correlated speed-dependent Keilson–Storer (pcSDKS) model has been proposed to describe H_2O line shapes [17]. Comparisons between simulated and experimental spectra have shown excellent agreements, thus demonstrating the existence of a partial correlation between velocity-changing and dephasing collisions [18]. Due to its complexity and large computational cost, the pcSDKS model has not been implemented into a fitting procedure. Instead, it has been used as a bench-mark to test the validity of simplified semiclassical models. This study has identified the partially correlated speed-dependent hard collision (pcSDHC) profile as the most appropriate model for self-colliding water molecules [18]. Exploiting these outcomes in the spectral analysis of high-quality water spectra, which have been acquired in a second-generation DBT experiment using a highly-precise dual-laser absorption spectrometer at 1.39 μm [19], we have succeeded in providing a new value for k_B with a combined uncertainty of 24 parts over 10^6 [20]. This is the best result obtained so far by using an optical method, its uncertainty being a factor of six smaller with respect to the one of Ref. [21].

In the present paper, we report complementary information regarding our new determination of the Boltzmann constant, with a particular focus on the line shape problem. The complete uncertainty budget is also discussed in details.

2. Experimental setup

The dual-laser water spectrometer is depicted in Fig. 1. It is based upon the use of a pair of offset-frequency locked extended-cavity diode lasers. One of the two lasers (the master laser, ML) acts as reference oscillator, while the second laser (the slave laser, SL) is actively controlled so that its emission frequency maintains a given offset with respect to the frequency of the reference laser. The ML, emitting in the wavelength range from 1.38 to 1.42 μm, has a maximum output power of 35 mW. It is frequency stabilized against the central frequency of a Lamb-dip, resulting from the nonlinear interaction that occurs inside a high-finesse optical resonator, in coincidence with the $4_{4,0} \rightarrow 4_{4,1}$ line of the $H_2{}^{18}O$ $\nu_1 + \nu_3$ band, at 7198.988700 cm^{-1}. At this purpose, the optical cavity was filled with a ^{18}O-enriched water–vapor sample at low pressures (~5 Pa). Hence, the ECDL was firstly locked to one of the resonant modes of the high-finesse cavity by means of the Pound–Drever–Hall technique (PDH). Then, the cavity-mode frequency was actively stabilized against the center of the Lamb dip by using a dispersive signal, as provided by the first-derivative detection of the cavity transmission, after dithering the cavity resonance by means of a sinusoidal signal at 2 kHz. More specifically, the bandwidth of the PDH feedback loop was measured to be about 1 MHz, leading to a frequency noise reduction larger than 50 dB (for Fourier frequencies smaller than 10 kHz) and, consequently, to a narrowing of the emission width down to 30 kHz (for an observation time of 1 ms). On the other hand, the bandwidth of the second control loop, namely the one used to lock the cavity resonance to the sub-Doppler signal, was measured to be 150 Hz. The overall relative frequency stability of the reference oscillator resulted to be at a level of 10^{-13} for an integration time of 1 s [22].

The slave laser, probing the $H_2^{18}O$ line of interest (namely, the $4_{4,1} \rightarrow 4_{4,0}$ line of $\nu_1 + \nu_3$ band, at 7199.103190 cm^{-1}), was offset-frequency locked to the ML, following the scheme that is based upon the continuous detection of the beat note frequency between the two lasers, as described elsewhere [19]. The offset frequency was provided by a radio-frequency (rf) synthesizer, which in turn was phase-locked to a GPS-disciplined Rb-clock. The bandwidth of the control loop was measured to be of about 10 kHz. By continuously tuning the offset frequency, it was possible to perform highly linear and highly accurate frequency scans of the SL around a given center frequency. In the adopted configuration, SL scans were 3.1 GHz wide and resulted from 3100 steps of 1 MHz each, with a step-by-step acquisition time of 100 ms. The active control of the emission frequency of the probe laser allowed us to build an absolute and reproducible frequency scale underneath the absorption spectra, thus satisfying one of the main requirements for a low-uncertainty DBT implementation.

Another key ingredient of our spectrometer is the intensity stabilization of the probe laser, which allowed us to remove one of the most subtle source of systematic deviation, namely, amplitude variation in the background baseline. In fact, the intensity control feedback loop effectively compensates for any power variation associated to a laser frequency scan, also including the periodic modulation of the power arising from spurious etalon effects, as well as absorption from water molecules along the path of the beam in air. The intensity control system is based on an acousto-optic modulator (AOM), which is used as an actuator to continuously control the amount of laser power that is deflected from the primary beam to the first diffracted order, this latter beam being employed for the spectroscopic experiment. The frequency stability of the rf signal at 80 MHz, driving the AOM, is sufficiently high (~10^{-7} over 300 s) to avoid the possible contribution to the overall frequency jitter of the first order laser beam. Intensity stabilization at the level of 10^{-4} was achieved over a frequency scan as wide as 10 GHz, the bandwidth of the control loop being ~50 kHz.

Laser–gas interaction, under the linear regime, takes place in an isothermal cell operating at the temperature of the triple point of water (TPW). This latter system, extensively described elsewhere [12], is made of three cylindrical chambers, one inside the other, the inner one being the cell that is filled with the water vapor sample. In order to ensure acoustic and thermal insulation from the outside environment, the other two chambers are kept under vacuum conditions by means of a rotative pump. The cell body is an electro-polished stainless steel cylinder with a length of 15 cm. A series of anti-reflection coated optical windows allows the laser to pass through the chambers, so as to reach the absorption cell. The rear edge of the cell is equipped with a flat mirror so that the laser beam could pass four times through the cell before being

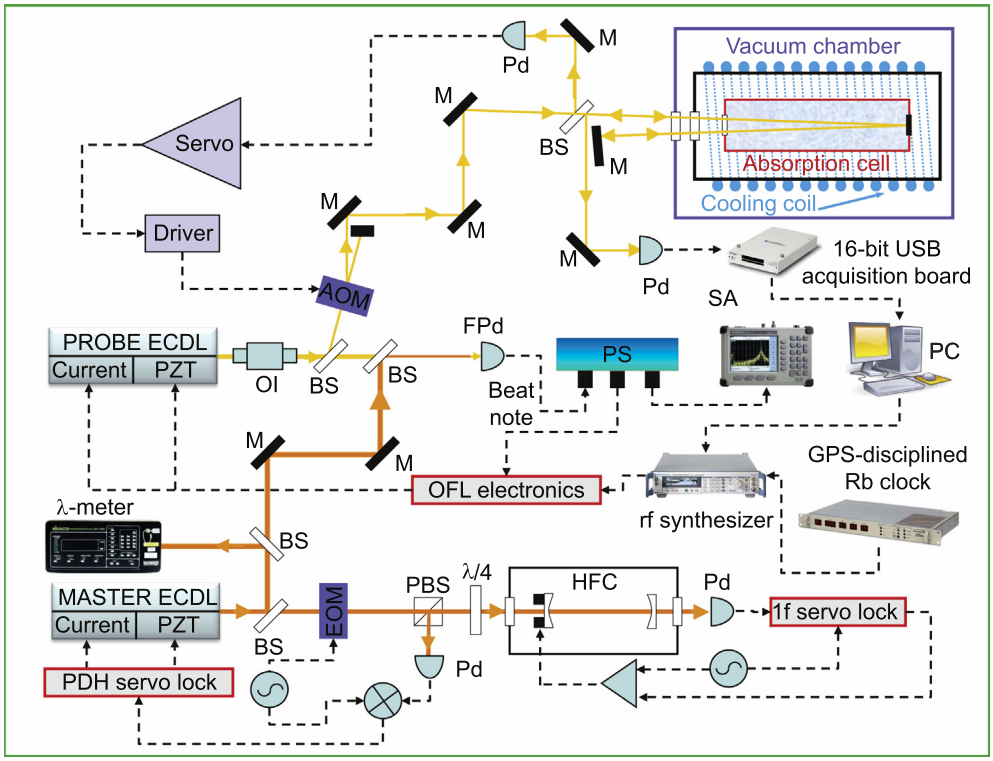

Fig. 1. Layout of the dual-laser absorption spectrometer. OI stands for optical isolator; BS, beam splitter; AOM, acousto-optic modulator; EOM, electro-optic modulator; $\lambda/4$, quarter wave plate; M, mirror; PBS, polarizing beam splitter; Pd, photodiode; FPd, fast photodiode; PS, radio frequency power-splitter; OFL, offset-frequency locking; HFC, high-finesse cavity; SA, spectrum analyzer; PC, personal computer.

probed by a ultralow-noise preamplified InGaAs photodiode (see the beam path drawn in Fig. 1). This latter exhibits a detection bandwidth of 1 kHz. An auxiliary thermostat is used for the first stage of temperature control, namely to bring the temperature of the cell slightly below the set-point. This is done by means of a cooling fluid circulating in a coil around the intermediate chamber. Hence, a constantan heater, uniformly wrapped around the cell, allows one to actively stabilize the temperature, thus reaching the desired value. Two capsule-type standard platinum resistance thermometers (SPRT) are inserted in the front and in the back of the cell at 180° between each other, in order to measure the temperature in two opposite points of the cell body. The two thermometers (Hart Scientific Model 5686) were calibrated at the TPW temperature by the Italian National Metrological Institute (INRIM). Their resistance is continuously measured with respect to a temperature stabilized standard resistor by means of an outstanding resistance bridge (ASL F18 Thermometry Bridge).

Prior to each measurement run, the isothermal cell was evacuated by means of a turbo molecular pump. Hence, it was filled with a 97.7% enriched ^{18}O water sample at variable pressures, ranging between 150 and 500 Pa, as measured by means of an absolute pressure gauge. The remaining 2.3% of the water sample included $H_2^{16}O$ (~2%) and $H_2^{17}O$ (~0.3%) molecules, other compounds and elements being present at trace amounts (between 1 and 10 ppm). We anticipate that narrowing effects are not expected to depend significantly on isotopic substitution. Similarly, gas purity is not an issue, as the collisional width is considered as a free parameter in the line fitting procedure.

Absorption spectra were acquired using a data acquisition board with a 16-bit resolution and a sampling rate of 1×10^6 samples per second. The possible nonlinearity of the whole detection chain was estimated to be well below the noise level. A LABVIEW code allowed us to control the whole setup, to perform step-by-step frequency scans and to acquire, for each step, the transmitted signal.

3. Line shape model

The power distribution $P(\omega)$, describing the shape of an isolated line centered at ω_0, is given by the following expression:

$$P(\omega) = (P_0 + P_1(\omega)) \exp\{-A \cdot \mathrm{Re}[S(\omega)]\} \quad (1)$$

where A represents the integrated absorbance, the parameters P_0 and P_1 account for a linear variation of the incident power, and Re[] stands for the real part of the quantity in square parenthesis. $S(\omega)$ is the complex line shape function that is strongly influenced by the collisional processes experienced by the absorbing molecules. This is, in turn, the sum of complex profiles, $F(\omega, \mathbf{v}_A)$, corresponding to absorbers with different velocities, $\mathbf{v}_A$, according to equation here below [23]:

$$S(\omega) = \int d\mathbf{v}_A F(\omega, \mathbf{v}_A). \quad (2)$$

The profile $F(\omega, \mathbf{v}_A)$ is determined by the probability distribution function of the absorbers, $f(\mathbf{r}, \mathbf{v}_A, t)$, which represents the fraction of molecules at time t, in a volume $d\mathbf{r}$ centered in $\mathbf{r}$, with a vectorial velocity between $\mathbf{v}_A$ and $\mathbf{v}_A + d\mathbf{v}_A$. This function satisfies the Boltzmann transport equation [24]. Therefore, under the impact approximation, it is possible to write:

$$F(\omega, \mathbf{v}_A) = \frac{1}{\pi} \int_0^\infty dt \int d^3\mathbf{r} f(\mathbf{r}, \mathbf{v}_A, t) \exp[i(\omega - \omega_0)t - i\mathbf{k} \cdot \mathbf{r} - (\Gamma(v_A) - i\Delta(v_A)t] \quad (3)$$

where $\mathbf{k}$ is the wave vector of the incident radiation, $\Gamma(v_A)$ and $\Delta(v_A)$ are the collisional width and shift of the line, respectively, and $v_A = |\mathbf{v}_A|$.

Speed dependence of collisional width produces a narrowing of the line, while speed dependence of collisional shifting leads to line asymmetry. In the formalism developed by Berman and Pickett

[25,26] collisional parameters are supposed to have a power-law dependence on the relative speed of the absorber/perturber system, with an exponent determined by the molecular interaction potential, which in turn is approximated by an inverse power form, namely, $V(r) \propto r^{-q}$, with $q = 3$, 4, 5, etc. respectively for a dipole–dipole, dipole–quadrupole, quadrupole–quadrupole, etc. interaction. As a result of a statistical average over the relative speeds, the collisional width and shift can be written as [27]:

$$\Gamma(v_A) = \frac{\Gamma_{av}}{(1+\alpha)^{m/2}} M\left(-\frac{m}{2}, \frac{3}{2}, -\alpha\left(\frac{v_A}{\bar{v}}\right)^2\right) \quad (4)$$

$$\Delta(v_A) = \frac{\Delta_{av}}{(1+\alpha)^{n/2}} M\left(-\frac{n}{2}, \frac{3}{2}, -\alpha\left(\frac{v_A}{\bar{v}}\right)^2\right) \quad (5)$$

with α, $\bar{v}$, m and n given by:

$$\alpha = \frac{m_p}{m_A} \quad \bar{v} = \sqrt{\frac{2k_B T}{m_A}} \quad m = \frac{q-3}{q-1} \quad n = -\frac{3}{q-1}. \quad (6)$$

In the equations above, Γ_{av} and Δ_{av} are the collisional width and shift, respectively, averaged over the absorbers' speed, $M(a,b,z)$ is the confluent hypergeometric function, while m_p and m_A are perturber and absorber masses. It is worth noting that the perturber-to-absorber mass ratio is equal to 1, since the perturber is identical to the absorber, in our experiment. Moreover, the natural linewidth has been neglected, being several orders of magnitude smaller than the collisional width.

The probability distribution function greatly determines the form of the line profile. In the simplest case, a free motion on straight-line trajectories is assumed for the absorbers, with a Maxwell distribution for their velocities, $W_M(\mathbf{v}_A)$. Therefore, it is possible to write:

$$f(\mathbf{r}, \mathbf{v}_A, t) = \delta(\mathbf{r} - \mathbf{v}_A t) W_M(\mathbf{v}_A), \quad (7)$$

where δ is the three-dimensional Dirac function. Using Eqs. (2), (3), and (7), the speed-dependent Voigt (SDV) profile can be obtained:

$$S_{SDV}(\omega) = \frac{1}{\pi} \int d\mathbf{v}_A \frac{W_M(\mathbf{v}_A)}{\Gamma(v_A) - i[\omega - \omega_0 - \Delta(v_A) - \mathbf{k}\cdot\mathbf{v}_A]}. \quad (8)$$

This model gives a simplified description of the line shape as it ignores the Dicke narrowing effect, which consists in a correction to the Doppler broadening caused by the averaging effect of velocity-changing collisions [28]. This physical process is usually modeled adopting either the soft collision or the hard collision approximation. Soft collision means that the effect of an individual collision is infinitesimal, so that many collisions are required to produce a significant change in velocity. In this case, the absorber motion becomes diffusive. Hence, $f(\mathbf{r},\mathbf{v}_A,t)$ obeys the diffusion equation, whose solution leads to the speed-dependent Galatry profile [27].

The hard collision limit assumes that each collision completely randomizes the velocity, according to a Maxwellian distribution. This approximation leads to the speed-dependent hard collision profile. In the partially correlated speed-dependent hard collision model, a correlation parameter η ($0 \leqslant \eta \leqslant 1$) is added to consider the partial correlation between velocity-changing collisions and dephasing collisions. This parameter η represents the fraction of dephasing collisions that provides also a velocity-changing effect, thus contributing to the Dicke narrowing. For the pcSDHC profile, we adopted the following form [29,30]:

$$S_{pcSDHC}(\omega) = \frac{1}{\pi} Re\left[\frac{G(\omega)}{1 - H(\omega)}\right] \quad (9)$$

where G and H are given by:

$$G(\omega) = \int d\mathbf{v}_A \frac{W_M(v_A)}{\beta(v_A) + \Gamma_D(v_A) - i[\omega - \omega_0 - \Delta_D(v_A) - \mathbf{k}\cdot\mathbf{v}_A]} \quad (10)$$

$$H(\omega) = \int d\mathbf{v}_A \frac{W_M(\mathbf{v}_A)[\beta(v_A) - \Gamma_{VD}(v_A) - i\Delta_{VD}(v_A)]}{\beta(v_A) + \Gamma_D(v_A) - i[\omega - \omega_0 - \Delta_D(v_A) - \mathbf{k}\cdot\mathbf{v}_A]}. \quad (11)$$

where the total collision rate is given by $\beta = \beta_v + \beta_{VD}$. The subscript V refers to purely velocity-changing collisions, D purely dephasing collisions, and VD simultaneous velocity-changing and dephasing collisions. Similarly, the collisional width and shift are given by $\Gamma = \Gamma_V + \Gamma_{VD}$ and $\Delta = \Delta_V + \Delta_{VD}$. Due to the physical meaning of the correlation parameter, it is possible to write $\beta_{VD} = \eta\beta$, $\Gamma_{VD} = \eta\Gamma$, and $\Delta_{VD} = \eta\Delta$. As far as the speed dependence is concerned, it is assumed to be identical for β and Γ and given by Eq. (4), while it is ignored for Δ, since we did not observe any asymmetry in the experimental profiles, at any pressure.

4. Results

Fig. 2 shows a few examples of absorption spectra, in coincidence with the $4_{4,1} \rightarrow 4_{4,0}$ line of the $H_2^{18}O$ $\nu_1 + \nu_3$ band, recorded at the TPW temperature as a function of the total gas pressure. At each of the pressure values, spectral acquisitions were typically repeated twenty times. The total number of acquired spectra, for the aims of the spectroscopic determination of k_B, was 718.

The pcSDHC model allowed us to successfully fit the measured spectral profiles within the experimental noise, which was measured to be of the order of 200 μV (root-mean-square fluctuations of the transmitted signal with empty cell). The fitting procedure was implemented under the MATLAB environment, using the trust region optimization algorithm, and involved a single spectrum at a time. Free parameters were A, P_0, P_1, Γ_{av}, Δ, β_{av} and $\Delta\omega_D$, β_{av} being the average collision frequency over molecular speeds. The center frequency, ω_0, was fixed at the extrapolated zero-pressure value of the line centers that were retrieved by fitting the absorption spectra to the symmetric version of the speed-dependent Voigt profile.

It is worth noting that the Doppler width is rather hidden in Eqs. (7)–(9) while it appears more clearly after the angular integration, with the polar axis along the wave vector [30]. The parameters η and q were fixed at 0.2 and 5.017, respectively. In setting the η value, we exploited the outcomes of Ref. [18], while the choice of the q value required a specific study. Firstly, setting a relatively small value for the q parameter ($q = 4.9$), the application of the fitting procedure to the spectra led to a linear trend in the retrieved k_B values, as a function of the gas pressure, with a negative slope. This situation obviously lacks physical meaning. Hence, the optimum q value could be identified only after repeatedly applying the fitting procedure to the whole set of spectra, each time setting

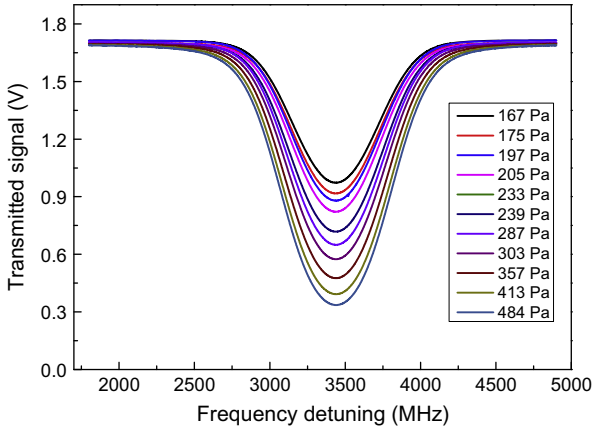

Fig. 2. Absorption line shape recorded at the TPW temperature and at different $H_2^{18}O$ pressures. The x-axis represents the frequency detuning from the center of the $4_{4,0} \rightarrow 4_{4,1}$ line of the $H_2^{18}O$ $\nu_1 + \nu_3$ band that is used for the absolute stabilization of ML.

a different value for the q parameter. In Fig. 3, we report the slopes that were retrieved from a weighted linear fit of the k_B data versus the integrated absorbance (which is proportional to the gas pressure), for different q values. A 2nd order polynomial fit of these slopes allowed us to retrieve the q parameter for which the slope is exactly zero. We found $q = 5.017 \pm 0.017$, which is consistent with that characteristic of a quadrupole–quadrupole interaction potential ($q = 5$). Fig. 4 shows the k_B values as a function of the integrated absorbance, resulting from the spectral analysis with $q = 5.017$. We note a growing fluctuation of the data points with decreasing pressures. This is caused by the decreasing signal-to-noise ratio in the recorded spectra that makes the statistical correlation between the free parameters, in the line fitting procedure, more effective. One might wonder which k_B values would have been retrieved by adopting a simplified model, such as the symmetric version of the speed-dependent Voigt profile. Fig. 5 reports the comparison between the two cases. Because of the lower number of free parameters (six, rather than seven), the statistical fluctuations from one spectrum to the other are significantly reduced when using the SDV model. Nevertheless, the k_B values are clearly underestimated, as line narrowing effects are not taken into account properly. It should be noted that also for the SDV fits the q value was fixed at the optimum one, namely, the value that gave a zero slope ($q = 4.785$). We also investigated the influence of the choice of the η value on the retrieved parameters in the pcSDHC fits. A very important outcome of this study is given by the fact that the retrieved Doppler and collisional widths do not depend on the selected η value, while β_{av} decreases with decreasing values of η, as clearly evidenced in Fig. 6. In our opinion, this is due to the fact that velocity-changing collisions do not give a large line-shape narrowing, which instead is mostly produced by the speed dependence of the relaxation rates [13]. Therefore, when setting a smaller physical correlation between velocity-changing and dephasing collisions, the Dicke narrowing effect appears even less effective. However, the importance of the η parameter to describe the physical situation of self-colliding water molecules can be confirmed. In fact, a zero value for η would lead to a negative slope in the linear dependence of the velocity-changing collision frequency on the gas pressure, circumstance that has no physical meaning.

Our spectroscopic determination of the Boltzmann constant results from the weighted mean of the values of Fig. 4, amounting to $(1.380631 \pm 0.000022) \times 10^{-23}$ J/K, the uncertainty being of the type A. Table 1 summarizes the complete uncertainty budget, which leads to a combined uncertainty of 24 ppm. This is a factor of 6 better than the result obtained by Lemarchand et al., from the analysis of 7171 spectra of NH_3 at 10.35 μm [21]. We should

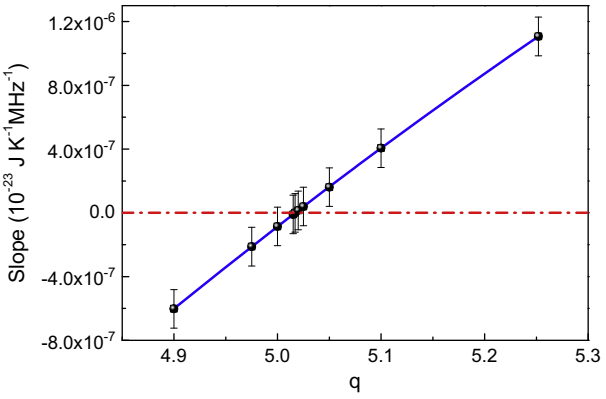

Fig. 3. Values of the slope retrieved from the weighted linear fit of k_B data versus the integrated absorbance, at different q exponents. The continuous blue line represents the 2nd order polynomial fit that provides the zero-slope condition.

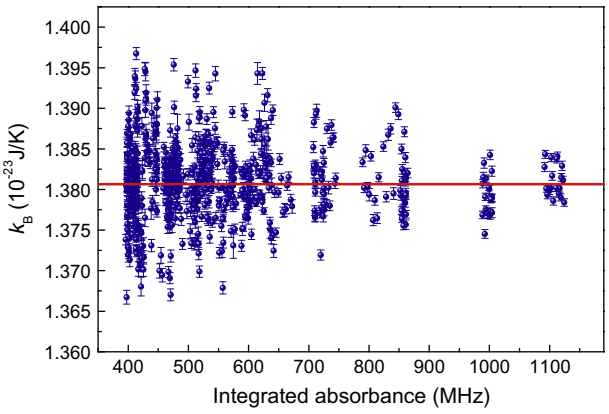

Fig. 4. Spectroscopic determination of the Boltzmann constant resulting from the analysis of 718 spectra by using the pcSDHC model with $q = 5.017$. Error bars, corresponding to one standard deviation, are the internal errors resulting from the fitting procedure. For comparison, the current CODATA value was drawn as a red line. (For interpretation of the references to color in this figure legend, the reader is referred to the web version of this article.)

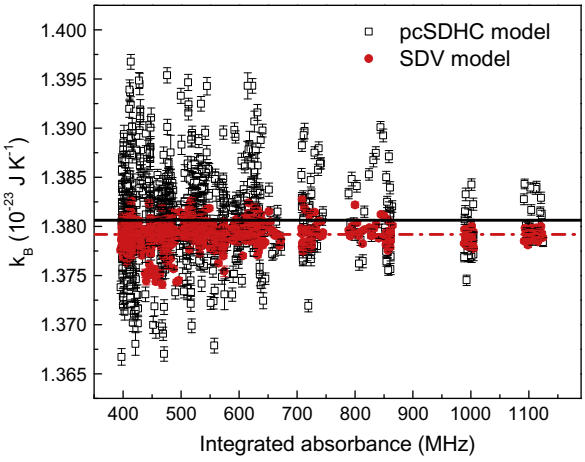

Fig. 5. Influence of the line shape model on the spectroscopic determination of k_B. The solid and the dash-dotted lines are the weighted means of the two datasets. The SDV model underestimates the Boltzmann constant.

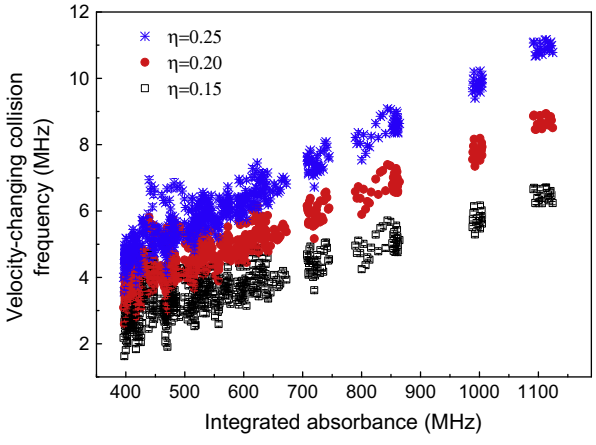

Fig. 6. Influence of the choice of the correlation parameter η on the retrieved velocity-changing collision frequency. For each of the three selected η values, a linear dependence of β_{av} on the integrated absorbance is clearly evidenced. The slope decreases with decreasing values of η and, for $\eta = 0.2$, well compares with the value that can be retrieved from diffusion theory.

mention that a revised analysis of the dataset of Ref. [31] (consisting of 1420 spectra in the pressure range between 0.1 and 1.3 Pa), as briefly discussed in Ref. [21], leaded to a determination of the Boltzmann constant with a global uncertainty of 50 ppm. This is surprising as the experiment of Ref. [21] exhibited several improvements with respect to that described in Ref. [31]. However, even when compared to this latter determination, our value gives an improvement by a factor of 2. Our determination is in agreement with the recommended CODATA value, namely, 1.3806488 (13) $\times 10^{-23}$ J/K. In the sub-sections that follow, we discuss the different sources of uncertainty. It is useful to remind that, according to the GUM (Guide to the expression of Uncertainty in Measurement), evaluations of uncertainty can be of the type A and type B: the former refers to a method of evaluation by statistical analysis of series of observations; the latter results from any means other than statistical analysis [32].

4.1. Temperature stability and uncertainty

The spectroscopic determination of the Boltzmann constant requires a highly accurate knowledge of the thermodynamic temperature of the absorbing gas. First of all, we tested the temperature stability of our cell by doing repeated determinations with a temporal resolution of 8 s, over a time span of about 9 h. The results are shown in the upper part of Fig. 7. A linear drift is clearly evidenced, amounting to -55×10^{-6} K/h. This translates into a stability of 0.11 mK over the time interval of 2 h that is typically required for doing twenty repeated spectral acquisitions. The Allan deviation analysis, reported in the lower part of the same figure, demonstrates a white-type fluctuation for integration times (τ) smaller than 500 s, characterized by a trend of the type $1/\tau^{0.5}$. Then, the Allan deviation starts to increase linearly with τ, thus confirming the occurrence of a linear drift. After applying the subtraction of the drift to the data of the upper panel of Fig. 7, it is possible to quote the statistical uncertainty on temperature measurements, amounting to 48×10^{-6} K (corresponding to one standard deviation) for an integration time of 8 s. When averaging over the time needed for the acquisition of a single spectrum (namely, 310 s), it reduces to $\sim 10^{-5}$ K and, therefore, can be completely neglected. In fact, its relative contribution to the budget of uncertainties on k_B amounts to 3.7×10^{-8}.

Possible temperature gradients along the cell were also investigated by doing repeated temperature readings at the two ends of the cell body, using the two SPRTs alternatively. As a result, the temperature uniformity was estimated to be at the level of 0.05 mK.

Finally, the overall uncertainty in temperature measurements was quoted considering the specifications of the resistance bridge, the uncertainty associated to the SPRT calibration at the TPW temperature, the correction that is applied to take into account the self-heating effect of the SPRTs, the uncertainty of the standard resistance, the temperature drift over the duration of a single spectral acquisition, and the temperature uniformity. As a result, we found 0.3 mK. This leads to a relative contribution to the uncertainty budget of 1.1×10^{-6}.

4.2. Frequency scale nonlinearity and uncertainty

The beat note between the two lasers, which was monitored by a spectrum analyzer, exhibited a signal-to-noise ratio of 40 dB in a 10 Hz resolution bandwidth. This was sufficient for direct counting. Therefore, in order to check the quality of the frequency scale, the beat note frequency was accurately measured by means of a universal counter with a gate time of 1 s, while scanning the offset-frequency locked slave laser over a frequency interval of 3.1 GHz. Fig. 8 shows the measured frequency as a function of the offset frequency, as provided by the rf synthesizer. A fit to a straight line is also shown. The fit residuals (computed as relative deviations between theory and experiment) demonstrate the excellent linearity of the frequency scan, possible deviations from the linearity being smaller than one part over 10^6 (namely, at the kHz level). This upper limit was set by the noise level in measuring the beat note frequency.

Similarly, the root-mean-square value of the relative deviations between measured and expected offset-frequencies amounts to $\sim 10^{-6}$. This gives the relative uncertainty on any value of the frequency axis underneath the absorption spectra and, consequently, translates into a relative uncertainty of the type B on the Boltzmann constant of 2×10^{-6}. Also in this case, the estimate gives an upper limit.

4.3. Line shape model

The uncertainty on the optimum q value, which was adopted in the analysis of the 718 spectra by using the pcSDHC model, contributes to the budget of uncertainties. In fact, we determined the variation of the weighted mean of the retrieved k_B values when

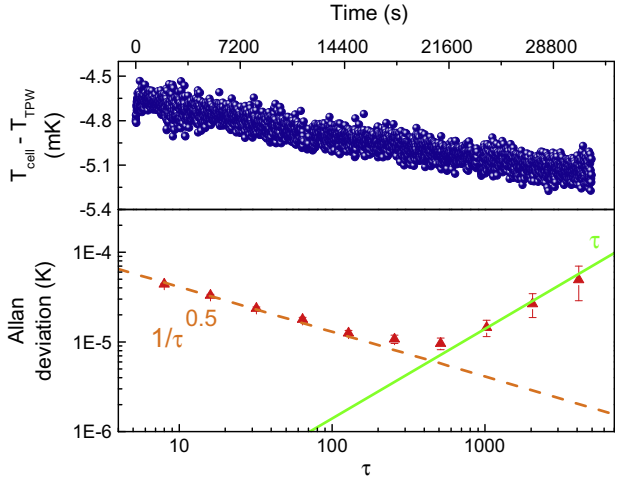

Fig. 7. Temperature stability test for the isothermal cell over a time span of nine hours. A linear drift of -1.55×10^{-8} K/s is measured. The Allan deviation analysis is shown in the lower panel. At low integration times ($\tau < 500$ s) white-type noise dominates. The influence of the linear drift becomes dominant for $\tau > 500$ s.

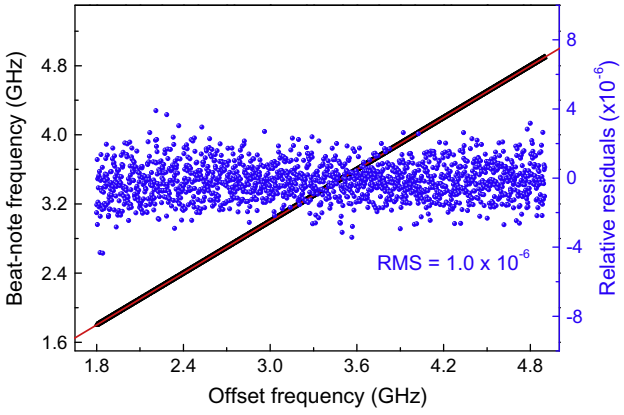

Fig. 8. Plot of the measured ML–SL beat note frequencies, for a probe laser scan across the $H_2^{18}O$ absorption line, along with a fit to a straight line. The offset frequencies set by the rf synthesizer are on the horizontal axis. Relative residuals exhibit a root-mean-square value of 1×10^{-6}.

varying the q parameter from 5 up to 5.034. This calculation led to a relative contribution of 14.9×10^{-6}.

4.4. Laser line emission width and FM broadening

In Section 2, we have shown that a modulation of the optical cavity length was necessary in order to build the absolute frequency reference. Unfortunately, this frequency dither was transferred from the master laser to the probe one, being the modulation frequency (2 kHz) well within the bandwidth of the offset-locking loop. As a result, a broadening of the emission width of the probe laser is expected. This effect was accurately investigated and quantified by using an optical frequency comb synthesizer, which is not displayed in Fig. 1 to avoid adding further complexity to the figure.

The comb is based upon a 100-MHz femtosecond Er:fiber oscillator (Toptica model FFS), with two phase-coherent amplified outputs: the one, centered at 1.55-μm wavelength, delivers nearly 250 mW of average power, while the other provides nearly 160 mW of supercontinuum (SC) light, whose spectral extension can be tuned by modification of the chirp of the pulses injected in the SC fiber. The comb can cover a spectral region as wide as ~150 THz, roughly corresponding to the 1030–2100 nm range.

Using an electrical spectrum analyzer, we recorded the beat note between the offset-frequency locked slave laser and the nearest tooth of the comb, varying the dither amplitude on the master laser. As shown in the inset of Fig. 9, the shape of the beat note is well reproduced by a Voigt convolution. Hence, a nonlinear least-squares fit of the beat note yielded the laser width (FWHW), whose values as a function of the dither amplitude are shown in Fig. 9. Obviously, we exploited the fact that the width of the comb tooth could be neglected (being at the kHz level). Reducing the dither, the laser width decreased down to the minimum value of about 1 MHz, with a Gaussian component of about 850 kHz and a Lorentzian one of about 210 kHz. This study allowed us to identify the optimum operation conditions for the aims of the spectroscopic experiment. Furthermore, it was possible to quantify the influence of the laser instrumentation function on the absorption profile of the molecular transition of interest. In fact, following the approach of Ref. [33], we simulated typical absorption spectra (in the thermodynamic conditions of our experiment) by doing the convolution between the laser profile, identical to the one emerging from the Voigt fit of Fig. 9, and the exponential of a SDV profile, setting the parameters equal to the expected ones. Then, the simulated spectra were analyzed by doing fits to Eq. (1), adopting the SDV model and ignoring the laser profile. So doing, it was possible to quantify the influence of the laser profile on the determination of the Doppler width and, consequently, of k_B. We found a relative contribution of the type B amounting to about 10 ppm.

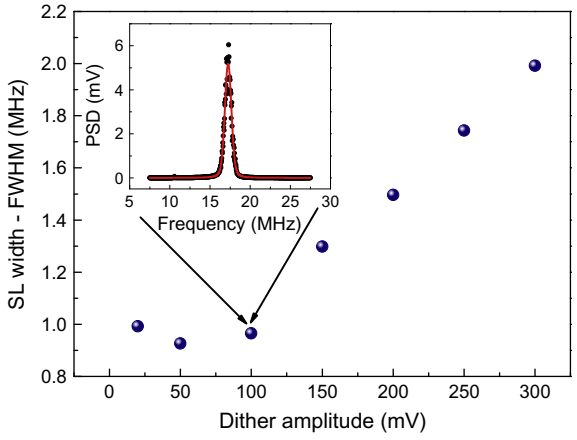

Fig. 9. Dependence of the SL emission width on the amplitude of the 2-kHz sinusoidal dither applied to the ML. The inset shows the power spectral density (PSD) of the beat note (observed with a resolution bandwidth of 10 Hz) between the optical frequency comb synthesizer and the SL, setting the dither amplitude at 100 mV. A fit to a Voigt convolution (red line) is also shown. (For interpretation of the references to color in this figure legend, the reader is referred to the web version of this article.)

4.5. Other components

Among the other sources of uncertainty, hyperfine structure (HFS) effects should be considered.

In fact, a hyperfine structure is expected as the selected transition is of the ortho type (namely, the total nuclear spin of the two hydrogen atoms is equal to 1) [34]. Nevertheless, HFS splitting, caused by spin–spin and spin–rotation interactions, is calculated to be more than one order of magnitude smaller than the emission width of the probe laser. We remind that the quadrupole moment of the hydrogen and oxygen (either ^{16}O or ^{18}O) nuclei is zero. Therefore, we estimate a relative contribution to the uncertainty budget much smaller than 10^{-6}. Similarly, we could completely ignore any effect due to a possible saturation of the line, as the maximum intensity of the probe laser along the beam path in the absorbing sample was calculated to be about 15 W/m^2, which is roughly eight orders of magnitude smaller than the saturation intensity of our line, as calculated at the pressure of 100 Pa by using the transition dipole moment and the self-broadening coefficient reported in the HITRAN database [35] and the equations of Ref. [36].

As for the measurement of the line center frequency, which enters into the determination of the Boltzmann constant, we used a 7-digit wavemeter (Burleigh, model WA1500), whose wavelength uncertainty, at 1.39 μm, corresponds to 30 MHz. This gives a relative contribution of 0.278×10^{-6}, as shown in the budget of Table 1.

As already mentioned, the possible non-linearity of the detection chain was estimated to be well below the noise level on the recorded spectra. In this respect, it is worth noting the excellent linearity in the response of InGaAs detectors (better than 10^{-3} over the large photocurrent range between 10^{-7} and 10^{-4} A), as document in the past literature [37]. Attempts to measure a possible nonlinearity by comparing absorption spectra acquired under the same experimental conditions, with the only exception of the power impinging the detector (which was attenuated by using a variable filter placed on the beam path between the cell and the detector), did not show any sign of deviation from linearity. Similarly, experimental profiles were not perturbed by spurious amplitude modulations of the laser beam, which were completely cancelled by the intensity control feedback loop.

Table 1
Uncertainty budget (in terms of relative contributions, corresponding to one standard deviation) related to the spectroscopic determination of the Boltzmann constant.

Component	Type A	Type B
Repeatability of Doppler width measurements	15.7×10^{-6}	
Frequency scale		$<2 \times 10^{-6}$
Line-center frequency		0.278×10^{-6}
Line emission width and FM broadening		10×10^{-6}
Saturation broadening		Negligible
Detector nonlinearity		Negligible
AM modulation effects		Negligible
Cell's temperature	3.7×10^{-8}	1.1×10^{-6}
Hyperfine structure effects		$<10^{-6}$
Line shape model		14.9×10^{-6}
Combined relative uncertainty = 24×10^{-6}		

Finally, no additional broadening is expected by the finite transit time of the $H_2^{18}O$ molecules through the laser beam, provided that the absorbing medium is homogeneous and isotropic, as demonstrated in Ref. [38].

5. Conclusions

We have reported on recent advances towards the development of low-uncertainty Doppler broadening thermometry, based upon precision molecular spectroscopy in the near-infrared region, for the aims of the spectroscopic determination of the Boltzmann constant. The dual-laser approach enabled us to reach unprecedented fidelity in the observation of the shape associated to a given vibration–rotation transition of water. A major effort in our work was devoted to line shape modeling, which is far from being trivial for self-colliding water molecules. In this respect, we have shown that the choice of the semiclassical model is of the utmost importance. In fact, a simplified model, such as the speed-dependent Voigt profile, can lead to a systematic deviation in the retrieval of k_B. The choice of the partially correlated speed-dependent hard collision profile, suggested by recent theoretical and experimental studies [17,18], revealed to be right, despite the complexity of the model. In fact, the retrieved k_B values did not show any dependence on the selected value of the correlation parameter. Furthermore, it was possible to find the optimum q exponent so as to reach the zero-slope condition. The uncertainty budget shows that the achievement of a global uncertainty at the ppm level, for the spectroscopic determination of k_B, is a realistic possibility.

The statistical uncertainty can be reduced by increasing the number of spectra, possibly enlarging the pressure interval. The limitation arising from FM broadening has been already removed. In fact, very recently, we have implemented noise-immune cavity-enhanced optical heterodyne molecular spectroscopy (NICE-OHMS) for the highly sensitive detection of the sub-Doppler line, on which the reference laser is stabilized [39]. In this respect, we benefit from the fact that NICE-OHMS provides a dispersion signal without dithering the optical cavity. As for the uncertainty associated to the line shape model, we believe that it will be significantly reduced once a global analysis approach will be used to simultaneously fit a manifold of profiles across a given range of pressures, sharing a restricted number of unknown parameters, including q and $\Delta\omega_D$. This approach would also reduce fluctuations resulting from statistical correlations among free parameters, as clearly demonstrated in Ref. [40].

Acknowledgments

This research was carried out in the framework of the EMRP Project No. SIB01-REG3 within the InK project (Implementing the new Kelvin, coordinated by Graham Machin, NPL, UK). The EMRP is jointly funded by the EMRP participating countries within EURAMET and the European Union.

References

[1] M. Planck, Theorie der Wärmestrahlung, Barth, Leipzig, 1921.
[2] Max Planck – Nobel Lecture: The Genesis and Present State of Development of the Quantum Theory. Nobelprize.org. Nobel Media AB 2013.
[3] BIPM 2011 Résolutions adoptees par la Conférence Générale dei Poids et Measures (24éme reunion) <http://www.bipm.org/utils/common/pdf/24_CGPM_Resolutions.pdf>.
[4] J. Fischer, S. Gerasimov, K.D. Hill, G. Machin, M.R. Moldover, L. Pitre, P. Steur, M. Stock, O. Tamura, H. Ugur, D.R. White, I. Yang, J. Zhang, Int. J. Thermophys. 31 (2007) 1753–1765.
[5] M. de Podesta, R. Underwood, G. Sutton, P. Morantz, P. Harris, D.F. Mark, F.M. Stuart, G. Vargha, G. Machin, Metrologia 50 (2013) 354–376.
[6] B. Fellmuth, J. Fischer, C. Gaiser, O. Jusko, T. Priruenrom, W. Sabuga, T. Zandt, Metrologia 50 (2013) L7–L11.
[7] C.J. Bordé, Metrologia 39 (2002) 435–463.
[8] C. Daussy, M. Guinet, A. Amy-Klein, K. Djerroud, Y. Hermier, S. Briaudeau, C.J. Bordé, C. Chardonnet, Phys. Rev. Lett. 98 (2007) 250801.
[9] G. Casa, A. Castrillo, G. Galzerano, R. Wehr, A. Merlone, D. Di Serafino, P. Laporta, L. Gianfrani, Phys. Rev. Lett. 100 (2008) 200801.
[10] K. Djerroud, C. Lemarchand, A. Gauguet, C. Daussy, S. Briaudeau, B. Darquié, O. Lopez, A. Amy-Klein, C. Chardonnet, C.J. Bordé, C. R. Phys. 10 (2009) 883–893.
[11] A. Castrillo, G. Casa, A. Merlone, G. Galzerano, P. Laporta, L. Gianfrani, C. R. Phys. 10 (2009) 894–906.
[12] A. Merlone, F. Moro, A. Castrillo, L. Gianfrani, Int. J. Thermophys. 31 (2010) 1360–1370.
[13] M.D. De Vizia, F. Rohart, A. Castrillo, E. Fasci, L. Moretti, L. Gianfrani, Phys. Rev. A 83 (2011) 052506.
[14] M.D. De Vizia, L. Moretti, A. Castrillo, E. Fasci, L. Gianfrani, Mol. Phys. 109 (2011) 2291–2298.
[15] M.D. De Vizia, A. Castrillo, E. Fasci, L. Moretti, F. Rohart, L. Gianfrani, Phys. Rev. A 85 (2012) 062512.
[16] L. Gianfrani, J. Phys.: Conf. Ser. 397 (2012) 012029.
[17] N.H. Ngo, H. Tran, R.R. Gamache, J. Chem. Phys. 136 (2012) 154310.
[18] H. Tran, N.H. Ngo, J.-M. Hartmann, R.R. Gamache, D. Mondelain, S. Kassi, A. Campargue, L. Gianfrani, A. Castrillo, E. Fasci, F. Rohart, J. Chem. Phys. 138 (2013) 034302.
[19] A. Castrillo, E. Fasci, G. Galzerano, G. Casa, P. Laporta, L. Gianfrani, Opt. Express 18 (2010) 21851–21860.
[20] L. Moretti, A. Castrillo, E. Fasci, M.D. De Vizia, G. Casa, G. Galzerano, A. Merlone, P. Laporta, L. Gianfrani, Phys. Rev. Lett. 111 (2013) 060803.
[21] C. Lemarchand, M. Triki, B. Darquié, C.J. Bordé, C. Chardonnet, C. Daussy, New J. Phys. 13 (2011) 073028.
[22] G. Galzerano, E. Fasci, A. Castrillo, N. Colluccelli, L. Gianfrani, P. Laporta, Opt. Lett. 34 (2009) 3107–3109.
[23] R. Ciurylo, Phys. Rev. A 58 (1998) 1029–1039.
[24] J.-M. Hartmann, C. Boulet, D. Robert, Collisional Effects on Molecular Spectra, Elsevier, 2008.
[25] P. Berman, J. Quant. Spectrosc. Radiat. Transfer 12 (1972) 1331–1342.
[26] H. Pickett, J. Chem. Phys. 73 (1980) 6090–6094.
[27] R. Ciurylo, J. Szudy, J. Quant. Spectrosc. Radiat. Transfer 57 (1997) 411–423.
[28] L. Galatry, Phys. Rev. 122 (1961) 1218–1223.
[29] A.S. Pine, J. Chem. Phys. 101 (1994) 3444–3452.
[30] A. Pine, J. Quant. Spectrosc. Radiat. Transfer 62 (1999) 397–423.
[31] C. Lemarchand, K. Djerroud, B. Darquié, O. Lopez, A. Amy-Klein, C. Chardonnet, C.J. Bordé, S. Briaudeau, C. Daussy, Int. J. Thermophys. 31 (2010) 1347–1359.
[32] ISO/TAG4/WG3, Guide to the Expression of Uncertainty in Measurement, International Organization for Standardization (ISO), Geneva, 1993.
[33] A.I. Nadezhdinskii, V.V. Plotnichenko, Y.Y. Ponurovskii, M.V. Spiridonov, Quantum Electron. 30 (2000) 87–93.
[34] C. Puzzarini, G. Cazzoli, M.E. Harding, J. Vázquez, J. Gauss, J. Chem. Phys. 131 (2009) 234304.
[35] L.S. Rothman, I.E. Gordon, Y. Babikov, A. Barbe, D. Chris Benner, P.F. Bernath, M. Birk, L. Bizzocchi, V. Boudon, L.R. Brown, A. Campargue, K. Chance, E.A. Cohen, L.H. Coudert, V.M. Devi, B.J. Drouin, A. Fayt, J.-M. Flaud, R.R. Gamache, J.J. Harrison, J.-M. Hartmann, C. Hill, J.T. Hodges, D. Jacquemart, A. Jolly, J. Lamouroux, R.J. Le Roy, G. Li, D.A. Long, O.M. Lyulin, C.J. Mackie, S.T. Massie, S. Mikhailenko, H.S.P. Müller, O.V. Naumenko, A.V. Nikitin, J. Orphal, V. Perevalov, A. Perrin, E.R. Polovtseva, C. Richard, M.A.H. Smith, E. Starikova, K. Sung, S. Tashkun, J. Tennyson, G.C. Toon, Vl.G. Tyuterev, G. Wagner, J. Quant. Spectrosc. Radiat. Transfer 130 (2013) 4–50.
[36] W. Ma, A. Foltynowicz, O. Axner, J. Opt. Soc. Am. B 25 (2008) 1144–1155.
[37] H.W. Yoon, J.J. Butler, T.C. Larason, G.P. Eppeldauer, Metrologia 40 (2003) S154–S158.
[38] C.J. Bordé, C. R. Phys. 10 (2009) 866–882.
[39] H. Dinesan, E. Fasci, A. Castrillo, L. Gianfrani, Opt. Lett. 39 (2014) 2198–2201.
[40] P. Amodio, L. Moretti, A. Castrillo, L. Gianfrani, J. Chem. Phys. 140 (2014) 044310.